Propagation of self-localized Q-ball solitons in the ^{3}He universe

S. Autti,[1,*] P. J. Heikkinen,[1,†] G. E. Volovik,[1,2] V. V. Zavjalov,[1] and V. B. Eltsov[1]
[1]*Low Temperature Laboratory, Department of Applied Physics, Aalto University, P.O. Box 15100, FI-00076 Aalto, Finland*
[2]*Landau Institute for Theoretical Physics, 142432 Chernogolovka, Russia*

(Received 31 August 2017; published 22 January 2018)

In relativistic quantum field theories, compact objects of interacting bosons can become stable owing to conservation of an additive quantum number Q. Discovering such Q balls propagating in the universe would confirm supersymmetric extensions of the standard model and may shed light on the mysteries of dark matter, but no unambiguous experimental evidence exists. We have created long-lived Q-ball solitons in superfluid ^{3}He, where the role of the Q ball is played by a Bose-Einstein condensate of magnon quasiparticles. The principal qualitative attribute of a Q ball is observed experimentally: its propagation in space together with the self-created potential trap. Additionally, we show that this system allows for a quantitatively accurate representation of the Q-ball Hamiltonian. Our Q ball belongs to the class of the Friedberg-Lee-Sirlin Q balls with an additional neutral field ζ, which is provided by the orbital part of the Nambu-Goldstone mode. Multiple Q balls can be created in the experiment, and we have observed collisions between them. This set of features makes the magnon condensates in superfluid ^{3}He a versatile platform for studies of Q-ball dynamics and interactions in three spatial dimensions.

DOI: 10.1103/PhysRevB.97.014518

I. INTRODUCTION

All self-bound macroscopic objects encountered in everyday life or observed experimentally are made from fermionic matter, while bosons mediate interactions between fermionic particles. Compact objects made purely from interacting bosons may, however, be stabilized in relativistic quantum field theory by conservation of an additive quantum number Q [1–3]. Observing such Q balls traveling in the universe would have striking consequences: Their discovery would support supersymmetric extensions of the standard model [4,5]; Q balls could have participated in baryogenesis [6] and formation of boson stars [7], and the dark matter [5,8–10] and supermassive compact objects in galaxy centers [11] may consist of Q balls. Nevertheless, unambiguous experimental evidence of Q balls has so far not been found in cosmology or in high-energy physics. In condensed-matter systems some analogs of Q balls have been theoretically suggested [12,13], while experimentally, properties of bright solitons in one-dimensional atomic Bose-Einstein condensates (BECs) [14] as well as those of Pekar polarons in ionic crystals [15] bear similarities to Q balls.

Here we present a laboratory realization, where the Q-ball Hamiltonian is accurately reproduced, unlike previously discussed qualitative analogs. Q balls are represented by Bose-Einstein condensates of magnon quasiparticles in superfluid ^{3}He, with the number of magnons N_{M} in the condensate playing the role of the charge Q and the frequency of precession of magnetization corresponding to the frequency of oscillation of the relativistic field within the Q ball. We experimentally demonstrate all essential features of a Q ball, including self-collection of bosons into a spontaneously formed trap, long lifetime, and propagation as a compact object in space.

Bose-Einstein condensation of quasiparticles, such as magnons [16,17], exciton-polaritons [18], and even photons [19], keeps extending the limits of known macroscopic coherent phenomena [20]. Quasiparticle condensates form a perspective platform for experimental studies of elusive systems and exotic theoretical models based on the tradition of quantum simulations in atomic BECs [21,22]. One of the most versatile environments is provided by the superfluid phases of ^{3}He, where a number of concepts from high-energy physics and cosmology have already been successfully tested [23–27]. Magnons in ^{3}He-B are quanta of transverse spin waves, accompanied by precessing magnetization of ^{3}He nuclei. Magnon condensation is manifested in the spontaneous phase coherence of the precession [16,28–31]. The lifetime of magnon condensates rapidly increases as temperature decreases below $\approx 3 \times 10^{-4}$ K and reaches minutes [32,33].

Magnons, carrying spin $-\hbar$, can be trapped within the sample volume using an appropriate profile of external magnetic field. An additional contribution to the trapping potential of magnon BEC originates from the spin-orbit interaction owing to the spatial distribution of the orbital anisotropy axis $\hat{\mathbf{l}}(\mathbf{r})$ of the superfluid ^{3}He-B order parameter. Unlike the common case of trapped atomic condensates, the magnon BEC is able to modify the underlying $\hat{\mathbf{l}}(\mathbf{r})$ profile and hence the confining potential [34,35]. It was proposed in Ref. [34] that this self-modification of the trap is an important prerequisite for the formation of a true, propagating Q ball. In earlier experiments, however, only condensates locked to preexisting traps with various degrees of self-modification were identified. Distinct from those, in our experiments the Q ball is formed when magnons, initially pumped by a radio-frequency pulse across the whole sample, collect on the periphery of the sample

*samuli.autti@aalto.fi
†Present address: Department of Physics, Royal Holloway, University of London, Egham, Surrey TW20 0EX, United Kingdom.

container in a self-created trap. This process spontaneously breaks the axial symmetry of the container-imposed $\hat{\mathbf{l}}(\mathbf{r})$ profile and of the applied magnetic field. Afterwards, the Q ball drifts towards the axis of the sample, as favored by the externally imposed fields, and the trap conforms to this movement. This propagation unambiguously demonstrates the nontrivial soliton nature of a true, long-lived Q ball. Moreover, we have created a second stationary Q ball at the sample axis and have observed how the propagating Q ball collides with the stationary one at the end of its track. We thereby show that the magnon BEC in ^{3}He-B allows for the most accurate condensed-matter representation of the nontopological Q-ball solitons in three dimensions.

II. MAGNON BEC AS Q BALL

The essential component of a Q ball is the relativistic complex field Φ of self-localized charge [1]. In the class of soliton solutions [3], which our experiment realizes, the Φ field interacts with the neutral scalar field ζ, which provides a confining potential. The Q balls in theories with only one scalar field Φ and the Q balls in theories with additional neutral field ζ are usually referred to as Q balls of the Coleman and Friedberg-Lee-Sirlin types, respectively. For a magnon Q ball in superfluid ^{3}He the field Φ is the transverse component of the coherently precessing spin, $\Phi \propto S_x + iS_y$. A quasiconserved number of magnons, $N_{\rm M} = \int dV(S - S_z)/\hbar$, becomes the Q charge. The Φ field in a Q ball obeys a relativistic Klein-Gordon equation [1,3]. In Appendix A we derive this equation for our magnon representation of Φ starting from the Leggett equations of spin dynamics in ^{3}He-B [Eq. (A8)]. We show that in the long-wavelength limit realized in the experiments it transforms to a Schrödinger equation

$$-i\hbar\frac{\partial\psi}{\partial t} = -\frac{\hbar^2}{2m}\Delta\psi + U(\mathbf{r})\psi, \tag{1}$$

where m is the magnon mass and $|\psi|^2 \propto |\Phi|^2$. The trapping potential $U(\mathbf{r})$ is formed by the magnetic field $|\mathbf{H}(\mathbf{r})| = \frac{2\pi}{|\gamma|}\nu_L(\mathbf{r})$ and the neutral field ζ of the Friedberg-Lee-Sirlin type:

$$U(\mathbf{r}) = U_H + U_{\rm text} \equiv h\nu_L(\mathbf{r}) + \frac{1}{2\pi\nu_L}\zeta^2(\mathbf{r}). \tag{2}$$

Here ν_L is the Larmor frequency, and γ is the gyromagnetic ratio of ^{3}He. The neutral field $\zeta(\mathbf{r})$ is provided by the Nambu-Goldstone mode of the orbital degrees of freedom, the texture of the $\hat{\mathbf{l}}$ vector, and is expressed in terms of β_L, the deflection angle of $\hat{\mathbf{l}}$ measured from $\mathbf{H} \parallel \hat{\mathbf{z}}$ [see Eq. (A25)]:

$$\zeta^2(\mathbf{r}) \propto \sin^2[\beta_L(\mathbf{r})/2]. \tag{3}$$

The condensate wave function ψ is normalized to the number of magnons $N_{\rm M}$ and can be expressed in terms of the tipping angle $\beta_{\rm M}$ of the precessing magnetization [see Eq. (A23)]:

$$\psi \propto \sin[\beta_{\rm M}(\mathbf{r})/2]e^{i\omega t}. \tag{4}$$

The frequency of the coherent precession $\omega = 2\pi\nu$ plays the role of the chemical potential of the magnon BEC. In relativistic theories it corresponds to the frequency of oscillation of the Φ field within the Q ball. For a detailed derivation of the above quantities, see Appendix A.

In the absence of magnons the spatial distribution of $\hat{\mathbf{l}}$ in our cylindrical container results from competing effects of the magnetic field and the container walls (see Fig 1): The orientation changes smoothly from parallel to the field at the container axis to perpendicular to the wall at the periphery.

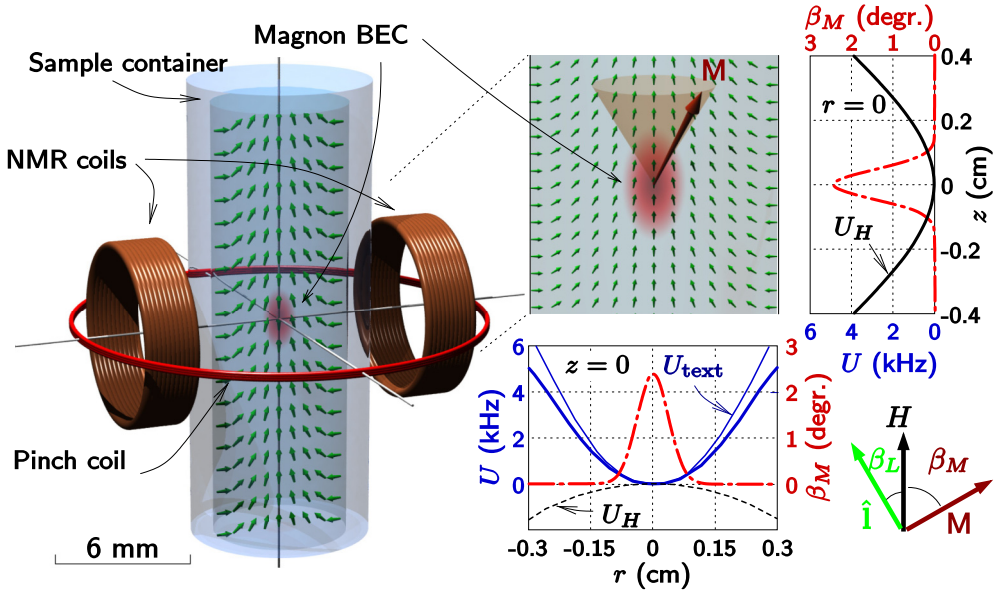

FIG. 1. Experimental setup: top part of the sample container, magnon condensate with precessing magnetization $\mathbf{M}$ (red blob) in a potential trap (thick solid lines), and corresponding wave functions for a small number of magnons (red dash-dotted lines). In the radial direction the potential minimum is formed by a combination of magnetic and textural energies, U_H and $U_{\rm text}$. In the axial direction the minimum is formed by the magnetic energy alone. Green arrows illustrate the spatial distribution of vector $\hat{\mathbf{l}}$, which is uniform in the $\hat{\mathbf{z}}$ direction in the absence of magnons. The pinch coil position defines $z = 0$, which corresponds also to the common axis of the NMR pickup coils. The potentials and wave functions are calculated for $T = 0.15T_{\rm c}$, $p = 0.5$ bar, and pinch coil current of 3 A.

Together with the magnetic potential, the profile of $\hat{\mathbf{l}}$ leads to a nearly harmonic three-dimensional potential [35]. We put the origin of our coordinate system at the bottom of this trap and choose $U(r=0,z=0)=0$. Therefore the condensate energy is conveniently measured as the shift $\Delta\nu$ of the precession frequency of the magnetization from the Larmor frequency at the origin: $\nu=\nu_L(r=0,z=0)+\Delta\nu$. All magnon states in this harmonic trap, including the ground state, have the frequency shift $\Delta\nu>0$. Relevant parts of the sample container, an example of the trapping potential, and the corresponding condensate wave function are shown in Fig. 1.

The Q-ball Hamiltonian in general contains a repulsive interaction between the charged and neutral fields. Here it arises from the spin-orbit interaction, which increases free energy by $F_{\rm so}=|\Phi(\mathbf{r})|^2\zeta^2(\mathbf{r})$. As the number of magnons increases, $\hat{\mathbf{l}}$ within the condensate reorients along $\hat{\mathbf{z}}$, reducing $U_{\rm text}(\mathbf{r})$ and the energy eigenstate in the trap. Experimentally, this is observed as a decrease in the condensate precession frequency ν with increasing signal amplitude. At large $N_{\rm M}$ the effect becomes so strong that $U_{\rm text}(\mathbf{r})$ forms a box [35] with a flat bottom and steep walls. This box is a bosonic analog of a hadron in the MIT bag model [36], as elaborated in Appendix B, and an essential prerequisite for formation of a Q ball.

III. OBSERVING Q BALLS IN EXPERIMENTS

In our experiments the superfluid ^{3}He sample, contained in a long, cylindrical quartz tube (diameter of 5.8 mm, length of 150 mm), is cooled down using a nuclear demagnetization refrigerator to (0.13–0.20)T_c. The experiments were carried out at $p=0.5$ bar (if not specified otherwise). The superfluid transition temperature T_c at $p=0.5$ bar is 1 mK. Temperature is measured using a quartz tuning fork sensitive to the thermal quasiparticle density in the sample [37,38]. The fork is located near the bottom of the container above the sintered connection to the nuclear demagnetization cooling stage. The applied magnetic field is 25.4 mT, and the corresponding nuclear magnetic resonance (NMR) frequency $\nu_L=\omega_L/2\pi=826$ kHz. In addition to the homogeneous axial field used for NMR, we use a pinch coil to create a field minimum along the sample container axis centered at $z=0$. The pinch coil produces also a small field maximum in the radial direction. The experimental setup and the magnetic field profile calibration are described in more detail in Refs. [33,39].

To monitor the formation and propagation of Q balls we use NMR techniques. They have proved powerful in probing various phenomena in ^{3}He close to zero temperature [33,40]. Magnons are pumped to the system with a radio-frequency pulse at a frequency above the ground-state frequency. The pumped magnons then quickly condense to the ground state, forming the BEC [16]. The coherently precessing magnetization of the condensate induces signal in the NMR pickup coils with amplitude $A\propto\int\sin\beta_M\,dV$. The frequency and amplitude of the recorded signal are extracted as a function of time by tracing the peak in a windowed Fourier transformation of the signal. For a fixed geometry of the condensate $A\propto N_{\rm M}^{1/2}$, but the proportionality coefficient depends strongly on the spatial distribution of the BEC wave function. This allows us to track the location of the Q ball in the measurements.

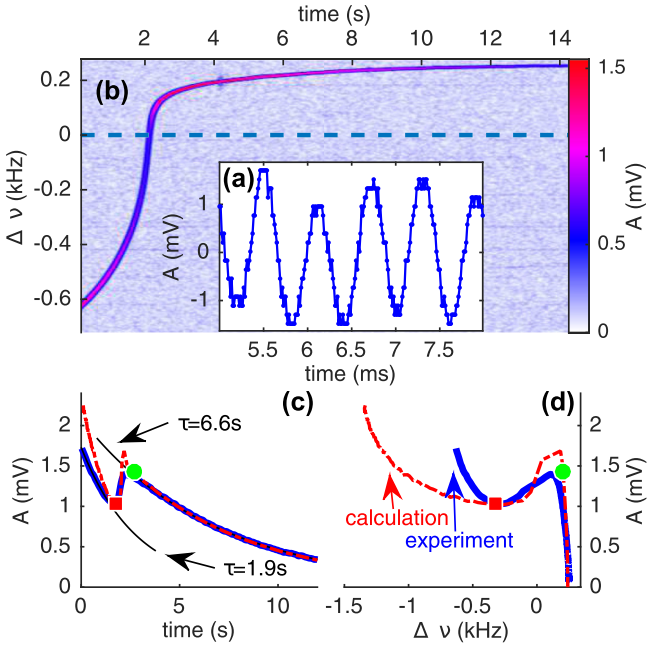

FIG. 2. Frequency and amplitude of a magnon Q ball during its decay: The Q ball is created by an rf pulse at $t=0$ ($T=0.15\,T_c$, $T_c\approx 1$ mK). (a) The signal recorded from the NMR pickup coils. (b) Windowed Fourier transform of the signal showing the magnon BEC as a sharp peak whose frequency shift $\Delta\nu$ and amplitude A change in time. (c) and (d) Measured (blue lines) and calculated (red dashed lines) dependencies, $A(t)$ and $A(\Delta\nu)$. Thin black lines in (c) are exponential fits to the measured decay. The initial decay time in the simulation is $\tau=1.7$ s. The red square and green circle mark the peripheral and central Q balls illustrated in Fig. 4.

IV. PROPAGATING Q BALL

After the exciting pulse is turned off at time $t=0$, $N_{\rm M}(t)$ decays slowly due to nonhydrodynamic spin diffusion and radiation damping [33], the former being the dominant contribution. If at $t=0$ the number of magnons $N_{\rm M}(0)$ is relatively small, the signal amplitude decays exponentially, $A(t)\propto\exp(-t/\tau)$, and the change in the frequency shift $\Delta\nu(t)$ during the decay is small [33,35]. With high $N_{\rm M}(0)>N_{\rm M}^{\rm c}\sim 10^{12}$, we observe reproducible decay signals with nonmonotonous $A(t)$ and $\Delta\nu(0)<0$; that is, ν is below the minimum of the original trapping potential (Fig. 2). The relaxation process is well defined: The relaxation follows a sequence of states which is independent of the relaxation rate, controlled by temperature, as demonstrated in Fig. 3(a). Decays started from different $N_{\rm M}(t)$ are identical after the common signal amplitude is reached [see Fig. 3(b)].

We explain these observations via formation of a peripheral magnon Q ball in a trap of spontaneously broken symmetry: Our self-consistent numerical simulation (details below) shows that with a sufficiently large $Q\equiv N_{\rm M}$ the textural potential $U_{\rm text}$ is suppressed due to the above-mentioned box effect. The radial maximum in the magnetic potential U_H allows the Q ball to self-localize in the periphery. Remarkably, the axial

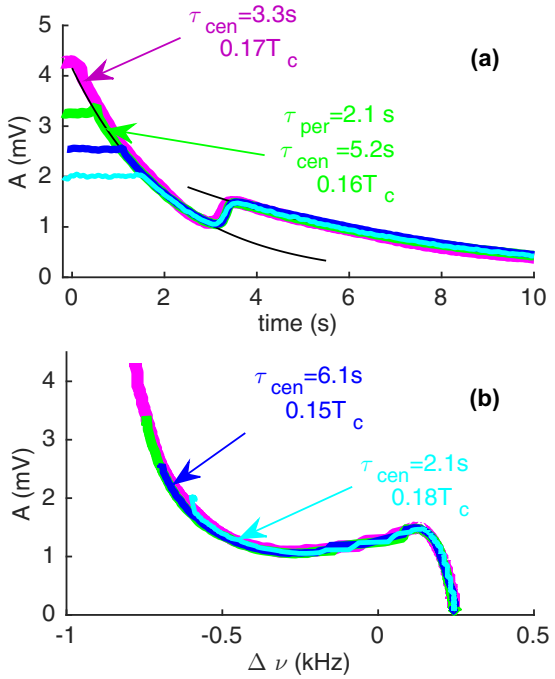

FIG. 3. (a) Q-ball decays and (b) corresponding frequency-amplitude dependencies at different temperatures and with different initial amplitudes at $p = 0$ bar. The measured decay signals are scaled in time according to $\tau_{\rm cen}$ to the units of the green (0.16 $T_{\rm c}$) line, revealing that the decay paths are identical in both $A(t)$ and $A(\Delta\nu)$. The signals begin with a nondecaying part of constant amplitude, where the condensate is supported by rf pumping ($t < 0$ in Fig. 2). In this plot $t = 0$ corresponds to turning off pumping for the magenta (0.17 $T_{\rm c}$) line, and other lines have been shifted in time in order to allow a comparison of the decay processes. $\tau_{\rm cen}$ stands for the time constant of exponential decay of the central Q ball (tail of the signal), and $\tau_{\rm per}$ stands for that of the peripheral one (beginning part of the signal). Thin black lines are exponential fits to the green (0.16 $T_{\rm c}$) line.

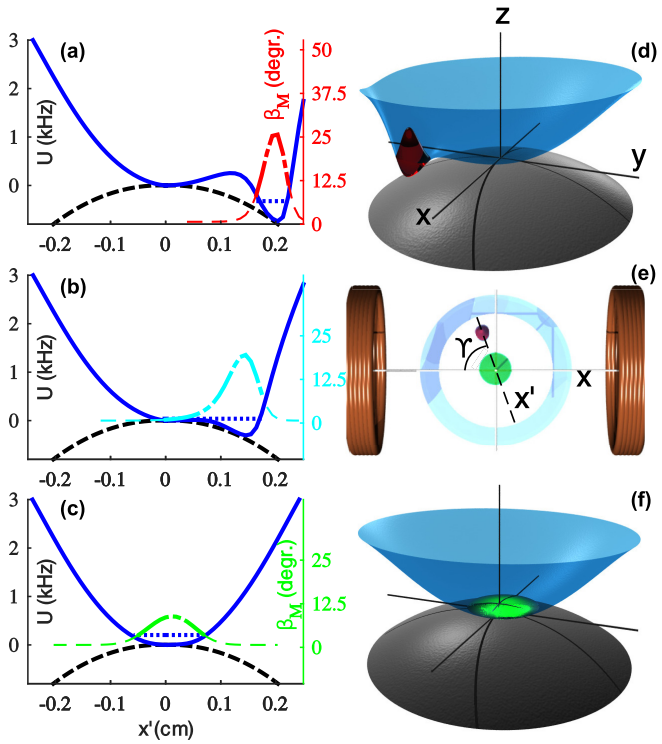

FIG. 4. Propagating magnon Q ball: (a) The peripheral Q ball, as marked in Fig. 2 by a square, is plotted in terms of β_M at $z = 0$ along the direction of Q-ball movement, labeled x'. The thick dash-dotted line is used where the condensate frequency (level indicated by the dotted blue line) is above the total potential U (thick solid blue line), and the thin dashed line is used where it is below. The magnetic potential U_H is drawn with a thick dashed black line. (b) While propagating from the periphery to the axis, the Q-ball frequency crosses $\Delta\nu = 0$. (c) The Q-ball state at the axis, marked in Fig. 2 by a circle. (d) and (f) The parts of the peripheral and central Q-ball wave functions (compact red and green blobs) that correspond to Q-ball frequency being above the total potential (lighter blue surface) are plotted in the $z = 0$ plane to illustrate the broken azimuthal symmetry of the peripheral state. The magnetic part of the potential is shown by a darker gray surface. (e) The top view of the sample container, the NMR coils, and the two Q-ball states [as plotted in (d) and (f)] reveals the time evolution of the Q-ball size. The peripheral Q ball is plotted traveling to one of the four degenerate directions with respect to the NMR coils.

symmetry of the confinement is spontaneously broken as well, and the Q ball becomes also azimuthally localized. This phenomenon is unlike conventional spontaneous symmetry breaking, where the potential remains axisymmetric (Appendix C). At the periphery of the sample, the Q ball's energy is below the original trap minimum, and thus $\Delta\nu < 0$. In the simulations the Q ball moves further from the axis (that is, closer to the sample container wall) than in the experiments, and hence its frequency is lower. This is probably due to insufficient rigidity in the model's orbital texture, which keeps the Q ball from eventually colliding with the container wall. The simulation is compared with the experiment in Fig. 2 and interpreted in Fig. 4.

The soliton nature of the propagating Q ball is manifested during the decay: The Q ball decays while staying at the periphery until it reaches the critical charge $Q_{\rm c} = N_{\rm M}^{\rm c}$, after which it quickly propagates to the center and simultaneously changes shape. This is an experimental realization of the threshold $Q_{\rm c}$ discussed in Ref. [3]. Thereafter the exponential decay continues roughly at a three times slower rate. The nonmonotonic evolution of the signal amplitude is a signature of the propagation: The peripheral Q ball is strongly localized, that is, compressed in both azimuthal and axial directions due to the pressure of the surrounding texture. The central Q ball spreads wider [see Fig. 4(e)] and therefore produces a larger signal for a given number of magnons. On top of the relatively slow decay of $N_{\rm M}(t)$, the fast propagation is therefore seen as a sudden increase in the signal amplitude. The change in the wave function also explains the different relaxation rates of the peripheral and central Q balls: The relaxation is mainly due to spin transfer over the thermal quasiparticles in ^{3}He-B, which increases with gradients of the wave function [33]. Those are larger for the compressed peripheral state.

In the simulations we treat the decay of the Q ball as a sequence of quasiequilibrium states. This assumption is justified by the fact that in the experiments the observed sequence of states along the Q-ball decay is relaxation rate independent (Fig. 3). The limitations of this approach are

revealed in the modest overshoot in simulated signal amplitude when the Q ball moves to the center [Figs. 2(b) and 2(c)]. We solve for the charged field [Eq. (1)] and the neutral $\hat{\mathbf{l}}$ field for each N_{M}, varying N_{M} in steps. Self-consistency between ψ and $\hat{\mathbf{l}}$ is reached with a fixed-point iteration. Close to Q_{c} the fixed-point iteration becomes sensitive to the initial condition. We start the simulation from $N_{\mathrm{M}} \gg Q_{\mathrm{c}}$ and use the solution at the previous step as the initial condition for the next step. The $\hat{\mathbf{l}}$ profile is calculated in three dimensions by minimization of appropriate free energy [41,42] including interaction with the magnon condensate in Eq. (A26). Solving Eq. (1) when $N_M = 0$ is described in Ref. [33]. The time evolution of the Q ball in simulations is calculated by solving Eq. (7) in Ref. [33] for the relaxation rate of the Zeeman energy. The signal amplitude in simulations is scaled to fit the very tail of the decay of the experimental signal, where the decay is well understood [33].

The expected NMR signal from the precessing magnetization in the simulation is calculated using the known geometry of the coil system. The direction that the peripheral Q ball is moving to, that is, the angle Υ between axes x and x' in Fig. 4, is fitted, yielding $\Upsilon = 67^\circ$. This fitted value of Υ corresponds to four possible directions of the Q ball's movement due to the symmetry of the coil system. Closer to the coils their sensitivity is higher, and hence the peripheral Q ball would produce a roughly two times larger signal than observed should it travel towards one of the two coils ($\Upsilon = 0^\circ$) and an about 50% smaller signal if it traveled along the direction perpendicular to the common axis of the NMR coils ($\Upsilon = 90^\circ$). The signal produced by the central condensate does not depend on Υ. To control this symmetry breaking in the simulation, we introduce a small symmetry-violating perturbation in the simulated potential to lift the degeneracy without influencing the structure of the Q ball.

V. COEXISTENCE OF TWO Q BALLS

The spatial distribution and rigidity of the neutral field $\zeta(\mathbf{r})$ can be controlled by adding an array of quantized vortices by rotating the sample [40]. Rotating at 1 rad/s, we are able to create two coexisting spatially separated Q balls using a rf pulse with a wide enough spectrum (see Fig. 5). That is, in addition to the Q ball on the periphery of the sample container, there is another Q ball localized to the container axis. They are stable owing to increased rigidity of the neutral field separating them. Due to the magnetic field profile, the central Q ball has higher energy than the one on the periphery.

During relaxation the peripheral Q ball moves towards the sample container axis, and when the energies of the two Q balls are sufficiently close, they merge, forming a single magnon Q ball in the central trap. This process is not very regular and depends on, e.g., the phases and the initial amplitudes of the magnon BECs. The coexistence of two magnon Q balls will allow detailed studies of interactions between them, especially the Josephson effect between two Q balls in flexible traps [43]. In the future this setup can also be used, e.g., for a quantum simulation of the Penrose-type "gravitationally" induced wave function collapse [44].

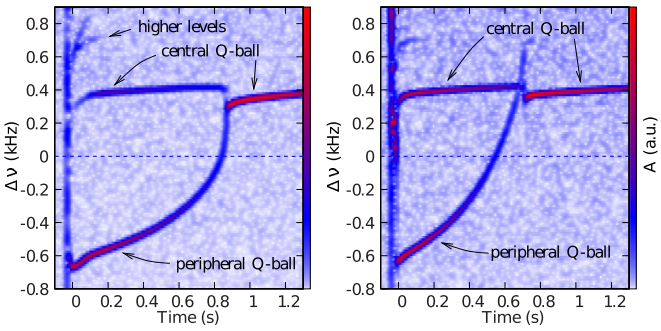

FIG. 5. Coexistence of central and peripheral Q balls: a true Q ball on the periphery of the sample container in the broken-symmetry trap and a central Q ball on the sample container axis (1 rad/s rotation, $T = 0.13\,T_c$). During the decay both eigenenergies (frequencies) increase, and when they become close enough, the condensates merge. This process of merging of two Q balls into a single one is demonstrated in two different experiments conducted under similar conditions. The panel on the left shows a straightforward merger, whereas on the right the peripheral Q ball goes through a metastable state: Just before the merger its energy is higher than that of the central Q ball. The metastability of the Q balls obtained by interaction of charged and neutral fields is discussed in Ref. [3]. Close to $t = 0$ some exited levels in the central trap are visible at higher frequencies.

VI. CONCLUSIONS

The concept of Q balls originates from high-energy physics and cosmology, where it has been used for so-far speculative explanations of many important phenomena in the universe, such as dark matter. We presented an experimental confirmation of the Q ball concept in a three-dimensional quantum simulation using a Bose-Einstein condensate of magnon quasiparticles in superfluid ^{3}He-B. This realization relies on the long lifetime of the magnons and their interaction with the orbital degrees of freedom of the underlying superfluid system. Both of these phenomena are also important from the point of view of BEC formation and spin superfluidity in general. The Q ball provides a new manifestation of the spin superfluidity of magnon BEC in ^{3}He-B, which complements the Josephson effect, quantized vorticity, superfluid spin currents, and the propagating Goldstone mode observed earlier in such condensates [16,45].

In our experiment the Q ball propagates over a macroscopic distance in the sample container, and the confining potential conforms to that movement. Such movement manifests the soliton nature of a true Q ball. We further demonstrate how this realization provides the possibility of creating two coexisting Q balls and observing how they interact and merge. A detailed study of the dynamics and interaction between the Q balls, such as the ac Josephson effect, remains an interesting task for the future.

ACKNOWLEDGMENTS

We thank V. V. Dmitriev, P. Skyba, and J. Nissinen for stimulating discussions. This work has been supported by the Academy of Finland (Project No. 284594). The work was carried out in the Low Temperature Laboratory, which is part of the OtaNano research infrastructure of Aalto University. P.J.H.

acknowledges financial support from the Väisälä Foundation of the Finnish Academy of Science and Letters and from the Finnish Cultural Foundation, and S.A. acknowledges that from the Finnish Cultural Foundation. The work by G.E.V. and V.B.E. was supported by the European Research Council (ERC) under the European Union's Horizon 2020 research and innovation program (Grant Agreement No. 694248).

APPENDIX A: DERIVATION OF Q-BALL REPRESENTATION BY MAGNON BEC

1. Magnons as relativistic particles

In what follows we derive the components of a magnon Q ball in detail. For further discussion of these topics, see Refs. [34,46].

Let us start from the spectrum of transverse spin-wave modes in ^{3}He-B in magnetic field,

$$\omega_\pm(k) = \pm\frac{\omega_L}{2} + \sqrt{\frac{\omega_L^2}{4} + k^2c^2}, \tag{A1}$$

where $\omega_L = \gamma H$ and c is the spin-wave velocity, which here is assumed to be isotropic for simplicity. The spectrum (A1) can be considered a spectrum of a relativistic particle with spin $S_z = \pm\hbar$ in an effective magnetic field:

$$E(S_z,k) = \sqrt{E_0^2 + k^2c^2} - \gamma\tilde{H}S_z. \tag{A2}$$

Here the rest energy E_0 of a particle is defined through its mass m as

$$E_0 = mc^2 = \frac{\hbar\omega_L}{2}, \tag{A3}$$

and the effective magnetic field is

$$\gamma\tilde{H} = \frac{\omega_L}{2}. \tag{A4}$$

At small k when $ck \ll \omega$, the spectrum transforms to that of the Galilean limit of a massive particle,

$$E(S_z = -\hbar,k) = \hbar\omega_L + \frac{\hbar^2k^2}{2m}, \tag{A5}$$

$$E(S_z = +\hbar,k) = \frac{\hbar^2k^2}{2m}. \tag{A6}$$

The mode with $S_z = -\hbar$ corresponds to optical magnons relevant to this work. They are called simply magnons throughout the text. Each magnon reduces the projection of spin on axis z by $\hbar$. The other branch ($S_z = \hbar$) is known as acoustic magnons [27].

The effective magnetic field can be removed by transformation to the spin reference frame rotating with angular velocity $\omega_L/2$. In this frame the spectrum of spin waves becomes

$$\tilde{E}(k) = \sqrt{E_0^2 + k^2c^2}. \tag{A7}$$

The relativistic spectrum of the spin waves suggests that magnons can be seen as quanta of a "relativistic" quantum field. Below we show that the field is a scalar field and magnons therefore play the role of the Φ field, which appears in high-energy physics as the core component of the Q-ball soliton. In what follows we set $\gamma = \hbar = 1$. Where relevant, these quantities are, however, expressed explicitly.

2. Deriving the relativistic spectrum

Let us write the linearized Leggett equations for spin dynamics in terms of the small spin-rotation angle $\boldsymbol{\theta}$, $|\boldsymbol{\theta}| \ll 1$, which is related to the deviation of spin density $\mathbf{S}$ from its equilibrium value $\chi\mathbf{H}$ [47]:

$$\mathbf{S} - \chi\mathbf{H} = \chi\,\partial_t\boldsymbol{\theta}. \tag{A8}$$

Here χ is the spin susceptibility.

The Lagrangian for the $\boldsymbol{\theta}$ field contains a linear term in the time derivative because the magnetic field violates time-reversal symmetry:

$$L = \frac{\chi}{2}[-(\partial_t\boldsymbol{\theta})^2 - (\boldsymbol{\theta}\times\partial_t\boldsymbol{\theta})\cdot\mathbf{H} + c^2\nabla_i\boldsymbol{\theta}\nabla_i\boldsymbol{\theta}] + F_{\rm so}(\boldsymbol{\theta}). \tag{A9}$$

The term $F_{\rm so}(\boldsymbol{\theta})$ is spin-orbit interaction. It originates from dipole-dipole interaction between spins of the particles forming a Cooper pair and violates spin-rotation symmetry. The Lagrangian (A9) can be rewritten in the following way:

$$L = \frac{\chi}{2}\left[-\left(\partial_t\boldsymbol{\theta} + \frac{1}{2}\boldsymbol{\omega}_L\times\boldsymbol{\theta}\right)^2 + E_0^2\boldsymbol{\theta}_\perp^2 + c^2\nabla_i\boldsymbol{\theta}\nabla_i\boldsymbol{\theta}\right] + F_{\rm so}(\boldsymbol{\theta}). \tag{A10}$$

If one ignores the spin-orbit coupling, this Lagrangian describes relativistic massive particles that interact with a SU(2) gauge field, whose time component is $a_0 = \frac{1}{2}\boldsymbol{\omega}_L$ [48,49].

Let us consider transverse NMR, where only the components $\boldsymbol{\theta}_\perp \perp \mathbf{H}$ are relevant (the static magnetic field is along the z axis). The gauge field is curvature free and can be eliminated, like above, by time-dependent rotation in spin space, which corresponds to the transformation to the spin reference frame rotating with angular velocity $\omega_L/2$. In this frame, both optical and acoustic modes are precessing with frequency $\omega_L/2$ in opposite directions and thus have the same energy $\tilde{E}$ in Eq. (A7).

The two-component real field (θ_x,θ_y) can be rewritten in terms of the scalar complex field Φ,

$$\Phi = \left(\frac{\chi}{2}\right)^{1/2}(\theta_x + i\theta_y). \tag{A11}$$

The Lagrangian (A10) becomes the Lagrangian for a scalar field interacting with a U(1) gauge field, whose time component is $A_0 = \omega_L/2$:

$$L = -(\partial_t\Phi + iA_0\Phi)(\partial_t\Phi^* - iA_0\Phi^*) + E_0^2|\Phi|^2 + c^2|\nabla\Phi|^2 + F_{\rm so}(\Phi,\Phi^*). \tag{A12}$$

In a constant magnetic field, the U(1) gauge is removed by introducing the time-dependent phase rotation, $\tilde{\Phi}(t) = \Phi(t)e^{iMt}$, and one obtains the Klein-Gordon Lagrangian for the complex relativistic scalar field used for the description of Q balls in high-energy physics:

$$L = -|\partial_t\tilde{\Phi}|^2 + E_0^2|\tilde{\Phi}|^2 + c^2|\nabla\tilde{\Phi}|^2 + F_{\rm so}(\tilde{\Phi},\tilde{\Phi}^*). \tag{A13}$$

In transverse NMR, where transverse components of spins precess with the Larmor frequency ω_L, the field $\tilde{\Phi}$ has the

form

$$\tilde{\Phi}(t) = \Phi(t)e^{iE_0 t} = \Phi_0 e^{-i\omega_L t}e^{iE_0 t} = \Phi_0 e^{-iE_0 t}. \quad \text{(A14)}$$

The energy spectrum of excitations of scalar field Φ in the absence of spin-orbit interaction is

$$\omega_\pm(k) = \pm\sqrt{E_0^2 + k^2c^2} - A_0, \quad \text{(A15)}$$

which corresponds to the spin wave spectrum in Eq. (A2). The branch with the minus sign gives the spectrum of optical magnons: $E(S_z = -1,k) = |\omega_-(k)|$.

The Lagrangian (A12) for the complex field in the absence of spin-orbit interaction has a conserved quantity, the U(1) charge Q:

$$Q = i\int d^3x(\tilde{\Phi}^*\partial_t\tilde{\Phi} - \tilde{\Phi}\partial_t\tilde{\Phi}^*). \quad \text{(A16)}$$

In the precessing state (A14) one obtains

$$Q = 2E_0\int dV|\Phi_0|^2 = \frac{\chi\omega_L}{2}\int dV\boldsymbol{\theta}_\perp^2 \approx \int dV(S - S_z), \quad \text{(A17)}$$

where we used $S_z = \sqrt{S^2 - S_\perp^2}$ and $S_\perp^2 = S^2\boldsymbol{\theta}_\perp^2$. Each magnon reduces the total spin by $\hbar$, and therefore the charge of the complex field coincides with the magnon number $N_{\rm M}$:

$$Q = N_{\rm M}. \quad \text{(A18)}$$

3. From the Klein-Gordon to Schrödinger equation

We have shown that the dynamics of magnetization obeys a relativistic Klein-Gordon equation, where the "speed of light" corresponds to the velocity of spin waves. The corresponding global U(1) symmetry is the $SO_S(2)$ symmetry under rotation of the spin system about the axis of applied constant magnetic field (axis z). The global U(1) charge Q comes from projection of spin along the direction of magnetic field, $Q = (S - S_z)/\hbar = N_{\rm M}$. This is a quasiconserved quantity in ^{3}He-B as magnons are long-lived quasiparticles.

The density of trapped magnons is relatively small, and the direct interaction between them is negligible compared with the interaction with the flexible orbital texture. Consider the nonrelativistic limit $kc \ll mc^2$ of the Klein-Gordon equation realized in the experiment. The wave vector k is the inverse of the characteristic length scale of the trapping potential $U(\mathbf{r})$. As in this limit one has

$$\frac{(\omega - A_0)^2 - E_0^2}{2E_0} \approx \omega - \omega_L, \quad \text{(A19)}$$

the Klein-Gordon equation for $\tilde{\Phi}$ transforms to the Schrödinger equation for ψ:

$$-i\hbar\frac{\partial\psi}{\partial t} = -\frac{\hbar^2}{2m}\Delta\psi + U\psi, \quad U(\mathbf{r}) = \hbar\omega_L(\mathbf{r}) + U_{\rm text}(\mathbf{r}). \quad \text{(A20)}$$

The Klein-Gordon wave function $\tilde{\Phi}$ is connected to the Schrödinger wave function ψ for magnons

$$\tilde{\Phi}(t) = \frac{\psi}{\sqrt{2E_0}}e^{iE_0 t - i\omega t}, \quad \int dV|\psi|^2 = N_{\rm M}, \quad \text{(A21)}$$

which satisfies $|\psi|^2 = \omega_L|\Phi|^2$, and is normalized to the number of magnons:

$$Q = i\int dV(\tilde{\Phi}^*\partial_t\tilde{\Phi} - \tilde{\Phi}\partial_t\tilde{\Phi}^*) = \int dV|\psi|^2 = N_{\rm M}. \quad \text{(A22)}$$

The Schrödinger wave function can be expressed in terms of the observables, phase $\alpha_{\rm M}$ and tipping angle $\beta_{\rm M}$ of the precessing magnetization:

$$\psi = \sqrt{\frac{2\chi H}{\gamma\hbar}}\sin(\beta_{\rm M}/2)\,\exp(i\omega t + i\alpha_{\rm M}). \quad \text{(A23)}$$

The nonrelativistic limit in Eq. (A6) of spectrum in Eq. (A2) is obtained solving Eq. (A20) for a free particle, assuming the frequency of precession is close to the Larmor frequency, $|\omega - \omega_L| \ll \omega_L$.

The potential $U(\mathbf{r})$ for magnons has two contributions: the spatial dependence of the local Larmor frequency $\omega_L(\mathbf{r}) = \gamma H(\mathbf{r})$ and that of the spin-orbit interaction $F_{\rm so}(\mathbf{r})$ in Eq. (A12) averaged over spin precession. The latter can be expressed in terms of the field of unit vector $\hat{\mathbf{l}}(\mathbf{r})$, defined as the direction of the orbital angular momentum of Cooper pairs in ^{3}He-B. The field of the $\hat{\mathbf{l}}(\mathbf{r})$ vector is time independent in the spin-precessing state:

$$F_{\rm so} = U_{\rm text}|\psi|^2, \quad \text{(A24)}$$

where

$$U_{\rm text}(\mathbf{r}) = \hbar\frac{2\Omega_B^2}{5\omega_L}[1 - l_z(\mathbf{r})] = \hbar\frac{4\Omega_B^2}{5\omega_L}\sin^2[\beta_L(\mathbf{r})/2] \equiv \frac{1}{\omega_L}\zeta^2(\mathbf{r}). \quad \text{(A25)}$$

Here $\Omega_B \ll \omega_L$ is the so-called Leggett frequency which characterizes the magnitude of the spin-orbit interaction [47], and β_L is the polar angle of the $\hat{\mathbf{l}}$ vector. The texture of the polar angle $\beta_L(\mathbf{r})$ plays the role of the neutral scalar field $\zeta(\mathbf{r})$ interacting with the complex field $\Phi(\mathbf{r})$ [or $\psi(\mathbf{r})$]. The texture $\zeta(\mathbf{r})$ is obtained by minimization of the textural energies [41,42] with the addition of the contribution which comes from the complex field of magnons [35]:

$$F_{\rm so} = \frac{1}{\omega_L}|\psi(\mathbf{r})|^2\zeta^2(\mathbf{r}) \equiv |\Phi(\mathbf{r})|^2\zeta^2(\mathbf{r}). \quad \text{(A26)}$$

APPENDIX B: MAGNON Q BALL AND MIT HADRON BAG

The magnon Q ball in ^{3}He-B is formed owing to the interaction between the magnon condensate described by the charged field Φ with conserved charge $Q = N_{\rm M}$ and the orbital field $\zeta(\mathbf{r})$, which is an analog of the neutral field [3,34]. The field $\zeta(\mathbf{r})$ forms a potential well in which the charge $Q = N_{\rm M}$ is condensed. In the process of self-localization the charged field $\Phi(\mathbf{r})$ locally modifies the neutral field $\zeta(\mathbf{r})$ via the spin-orbit interaction [Eq. (A26)]. That interaction is repulsive, and if the magnetic part of the trapping potential U_H is neglected, in the limit of large $N_{\rm M}$ a cavity is formed, which is void of neutral field $\zeta(\mathbf{r})$ and filled with the charge field $\Phi(\mathbf{r})$ (see Fig. 6). That is, the flexible textural trap $U_{\rm text}$ transforms to a box with walls impenetrable for magnons [35]. The pressure from the field ζ is compensated by the zero-point pressure of the free

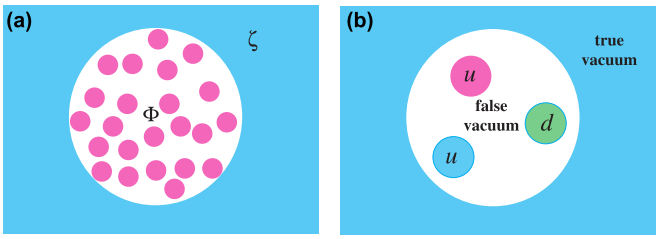

FIG. 6. Q ball in ^{3}He-B as a MIT hadron bag. (a) The BEC of magnons (magenta circles) in the limit of large N_M in a box cavity, which is void of neutral field and filled with the charge field $\Phi(\mathbf{r})$. (b) Simplified MIT bag model of hadrons, where the quarks forming a hadron are confined within a blob of a false-vacuum void of the actual vacuum of the QCD field.

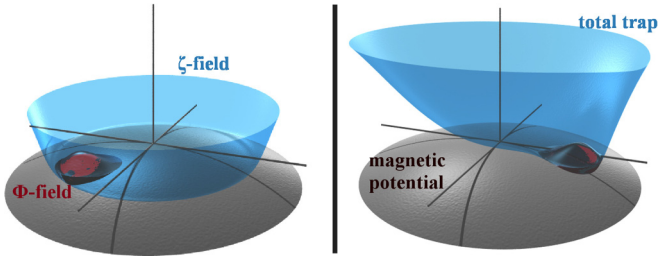

FIG. 7. Illustration of a conventional (left) and an unconventional (right) spontaneous breaking of global continuous symmetry: In the conventional situation, the potential acquires the form of a Mexican hat but remains axisymmetric. The trapped particle(s) becomes localized in one of the degenerate points in the valley of the potential, thus breaking the $U(1)$ symmetry. For the magnon Q ball the situation is different: The Mexican hat potential itself is unstable towards breaking of axial symmetry due to the self-trapping effect. The ζ field conforms to the movements of the magnon Q-ball soliton (Φ field).

magnons. This is an analog of the MIT bag model of hadrons, where the quarks forming a hadron are confined only within the QCD vacuum field and the quarks can freely move in the false-vacuum void of the QCD field [36]. The confined quarks form a blob of false vacuum, where the external pressure from the QCD vacuum is compensated by the zero-point pressure of the confined quarks.

APPENDIX C: SYMMETRY BREAKING

Let us compare the Q-ball formation with conventional symmetry breaking, such as the symmetry breaking which triggers the Higgs mechanism in the standard model [50]. In the conventional case the potential acquires the shape of a Mexican hat but remains axisymmetric as in the left panel of Fig. 7. In our case the potential $U_{\rm text}(\mathbf{r})$ does not have the Mexican-hat shape (Fig. 7, right panel). The potential shape depends on the density of bosons localized in it. Therefore the axisymmetric Mexican-hat potential itself is unstable towards symmetry breaking in the azimuthal coordinate. Although the generalized Hamiltonian for the combined Φ and $\hat{\mathbf{l}}$ fields remains symmetric (degenerate), in the Q-ball picture the potential $U_{\rm text}(\mathbf{r})$ is localized along the bosons. This is a unique experimental example of spontaneous breaking of the rotational SO(2) symmetry on top of formation of the axisymmetric Mexican-hat potential.

[1] S. Coleman, Q-balls, Nucl. Phys. B **262**, 263 (1985).
[2] A. Cohen, S. Coleman, H. Georgi, and A. Manohar, The evaporation of Q-balls, Nucl. Phys. B **272**, 301 (1986).
[3] R. Friedberg, T. D. Lee, and A. Sirlin, Class of scalar-field soliton solutions in three space dimensions, Phys. Rev. D **13**, 2739 (1976).
[4] A. Kusenko and M. Shaposhnikov, Supersymmetric Q-balls as dark matter, Phys. Lett. B **418**, 46 (1998).
[5] K. Enqvist and A. Mazumdar, Cosmological consequences of MSSM flat directions, Phys. Rep. **380**, 99 (2003).
[6] S. Kasuya and M. Kawasaki, Baryogenesis from the gauge-mediation type Q-ball and the new type of Q-ball as the dark matter, Phys. Rev. D **89**, 103534 (2014).
[7] C. Palenzuela, L. Lehner, and S. L. Liebling, Orbital dynamics of binary boson star systems, Phys. Rev. D **77**, 044036 (2008).
[8] S. Kasuya, E. Kawakami, and M. Kawasaki, Axino dark matter and baryon number asymmetry production by the Q-ball decay in gauge mediation, J. Cosmol. Astropart. Phys. **2016**, 011.
[9] E. Cotner and A. Kusenko, Primordial Black Holes from Supersymmetry in the Early Universe, Phys. Rev. Lett. **119**, 031103 (2017).
[10] A. Kusenko, V. Kuzmin, M. Shaposhnikov, and P. G. Tinyakov, Experimental Signatures of Supersymmetric Dark-Matter Q-Balls, Phys. Rev. Lett. **80**, 3185 (1998).
[11] S. Troitsky, Supermassive dark-matter Q-balls in galactic centers? J. Cosmol. Astropart. Phys. **2016**, 27.
[12] D. Hong, Q-balls in superfluid ^{3}He, J. Low Temp. Phys. **71**, 483 (1988).
[13] K. Enqvist and M. Laine, Q-ball dynamics from atomic Bose-Einstein condensates, J. Cosmol. Astropart. Phys. **2003**, 003.
[14] K. E. Strecker, G. B. Partridge, A. G. Truscott, and R. G. Hulet, Formation and propagation of matter-wave soliton trains, Nature (London) **417**, 150 (2002).
[15] J. T. Devreese and A. S. Alexandrov, Froehlich polaron and bipolaron: Recent developments, Rep. Prog. Phys. **72**, 066501 (2009).
[16] Y. M. Bunkov and G. E. Volovik, *Spin Superfluidity and Magnon Bose-Einstein Condensation*, in *Novel Superfluids*, edited by K. H. Bennemann and J. B. Ketterson (Oxford University Press, London, 2013), Vol. 1, pp. 253–311.
[17] S. Demokritov, V. Demidov, O. Dzyapko, G. Melkov, A. Serga, B. Hillebrands, and A. Slavin, Bose-Einstein condensation of quasi-equilibrium magnons at room temperature under pumping, Nature (London) **443**, 430 (2006).
[18] J. Kasprzak, M. Richard, S. Kundermann, A. Baas, P. Jeambrun, J. Keeling, F. Marchetti, M. Szymńska, R. André, J. Staehli, V. Savona, P. Littlewood, B. Deveaud, and L. Dang, Bose-Einstein condensation of exciton polaritons, Nature (London) **443**, 409 (2006).
[19] J. Klaers, J. Schmitt, F. Vewinger, and M. Weitz, Bose-Einstein condensation of photons in an optical microcavity, Nature (London) **468**, 545 (2010).

[20] D. A. Bozhko, A. A. Serga, P. Clausen, V. I. Vasyuchka, F. Heussner, G. A. Melkov, A. Pomyalov, V. S. L'vov, and B. Hillebrands, Supercurrent in a room-temperature Bose-Einstein magnon condensate, Nat. Phys. **12**, 1057 (2016).

[21] I. Bloch, J. Dalibard, and W. Zwerger, Many-body physics with ultracold gases, Rev. Mod. Phys. **80**, 885 (2008).

[22] I. M. Georgescu, S. Ashhab, and F. Nori, Quantum simulation, Rev. Mod. Phys. **86**, 153 (2014).

[23] G. E. Volovik, *The Universe in a Helium Droplet* (Oxford University Press, Oxford, 2003).

[24] W. H. Zurek, Cosmological experiments in superfluid helium? Nature (London) **317**, 505 (1985).

[25] V. M. H. Ruutu, V. B. Eltsov, A. J. Gill, W. B. Kibble, M. Krusius, Y. G. Makhlin, B. Placais, G. E. Volovik, and W. Xu, Vortex formation in neutron-irradiated superfluid ^{3}He as an analog of cosmological defect formation, Nature (London) **382**, 334 (1996).

[26] D. I. Bradley, S. N. Fisher, A. M. Guenault, R. P. Haley, J. Kopu, H. Martin, G. R. Pickett, J. E. Roberts, and V. Tsepelin, Relic topological defects from brane annihilation simulated in superfluid ^{3}He, Nat. Phys. **4**, 46 (2008).

[27] V. V. Zavjalov, S. Autti, V. B. Eltsov, P. J. Heikkinen, and G. E. Volovik, Light Higgs channel of the resonant decay of magnon condensate in superfluid ^{3}He, Nat. Commun. **7**, 10294 (2016).

[28] A. S. Borovik-Romanov, Y. M. Bun'kov, V. V. Dmitriev, and Y. M. Mukharskii, Long-lived induction signal in superfluid ^{3}He-B, JETP Lett. **40**, 1033 (1984).

[29] I. A. Fomin, Long-lived induction signal and spatially nonuniform spin precession in ^{3}He-B, JETP Lett. **40**, 1037 (1984).

[30] Y. M. Bunkov, S. N. Fisher, A. M. Guénault, and G. R. Pickett, Persistent Spin Precession in ^{3}He-B in the Regime of Vanishing Quasiparticle Density, Phys. Rev. Lett. **69**, 3092 (1992).

[31] S. Fisher, A. Guénault, A. Hale, G. Pickett, P. Reeves, and G. Tvalashvili, Thirty-minute coherence in free induction decay signals in superfluid ^{3}He-B, J. Low Temp. Phys. **121**, 303 (2000).

[32] S. N. Fisher, G. R. Pickett, P. Skyba, and N. Suramlishvili, Decay of persistent precessing domains in ^{3}He-B at very low temperatures, Phys. Rev. B **86**, 024506 (2012).

[33] P. J. Heikkinen, S. Autti, V. Eltsov, J. Hosio, M. Krusius, and V. Zavjalov, Relaxation of Bose-Einstein condensates of magnons in magneto-textural traps in superfluid ^{3}He-B, J. Low Temp. Phys. **175**, 3 (2014).

[34] Y. M. Bunkov and G. E. Volovik, Magnon Condensation into a Q Ball in ^{3}He-B, Phys. Rev. Lett. **98**, 265302 (2007).

[35] S. Autti, Y. M. Bunkov, V. B. Eltsov, P. J. Heikkinen, J. J. Hosio, P. Hunger, M. Krusius, and G. E. Volovik, Self-Trapping of Magnon Bose-Einstein Condensates in the Ground State and on Excited Levels: From Harmonic to Box Confinement, Phys. Rev. Lett. **108**, 145303 (2012).

[36] S. Autti, V. B. Eltsov, and G. E. Volovik, Bose analogs of MIT bag model of hadrons in coherent precession, JETP Lett. **95**, 544 (2012).

[37] R. Blaauwgeers, M. Blažková, M. Človečko, V. B. Eltsov, R. de Graaf, J. Hosio, M. Krusius, D. Schmoranzer, W. Schoepe, L. Skrbek, P. Skyba, R. E. Solntsev, and D. E. Zmeev, Quartz tuning fork: Thermometer, pressure- and viscometer for helium liquids, J. Low Temp. Phys. **146**, 537 (2007).

[38] M. Blažková, M. Človečko, V. B. Eltsov, E. Gažo, R. de Graaf, J. J. Hosio, M. Krusius, D. Schmoranzer, W. Schoepe, L. Skrbek, S. P., R. E. Solntsev, and W. F. Vinen, Vibrating quartz fork: A tool for cryogenic helium research, J. Low Temp. Phys. **150**, 525 (2008).

[39] V. V. Zavjalov, S. Autti, V. B. Eltsov, and P. J. Heikkinen, Measurements of the anisotropic mass of magnons confined in a harmonic trap in superfluid ^{3}He-B, JETP Lett. **101**, 802 (2015).

[40] V. B. Eltsov, R. de Graaf, M. Krusius, and D. Zmeev, Vortex core contribution to textural energy in ^{3}He-B below $0.4T_c$, J. Low Temp. Phys. **162**, 212 (2011).

[41] E. V. Thuneberg, Hydrostatic theory of superfluid ^{3}He-B, J. Low Temp. Phys. **122**, 657 (2001).

[42] J. Kopu, Numerically calculated NMR response from different vortex distributions in superfluid ^{3}He-B, J. Low Temp. Phys. **146**, 47 (2007).

[43] K. Nakata, K. A. van Hoogdalem, P. Simon, and D. Loss, Josephson and persistent spin currents in Bose-Einstein condensates of magnons, Phys. Rev. B **90**, 144419 (2014).

[44] R. Penrose, Gravitational Collapse and Space-Time Singularities, Phys. Rev. Lett. **14**, 57 (1965).

[45] E. Sonin, Spin currents and spin superfluidity, Adv. Phys. **59**, 181 (2010).

[46] G. E. Volovik, Twenty years of magnon Bose condensation and spin current superfluidity in ^{3}He-B, J. Low Temp. Phys. **153**, 266 (2008).

[47] D. Vollhardt and P. Wölfle, *The Superfluid Phases of Helium 3* (Dover, Mineola, NY, 2013).

[48] V. Mineev and G. Volovik, Electric dipole moment and spin supercurrent in superfluid ^{3}He, J. Low Temp. Phys. **89**, 823 (1992).

[49] B. W. A. Leurs, Z. Nazario, D. I. Santiago, and J. Zaanen, Non-Abelian hydrodynamics and the flow of spin in spin orbit coupled substances, Ann. Phys. (NY) **323**, 907 (2008).

[50] K. Nakamura *et al.*, Review of particle physics, J. Phys. G: Nucl. Part. Phys. **37** 075021 (2010).